Supporting Information

Theoretical Study of Photocatalytic Properties on 2D InX(X=S, Se)/Transition-metal Disulfides (MoS_2 and WS_2) Van der Waals Heterostructures

Hailing Guo,[a,#] Zhaofu Zhang,[b,#] Bingquan Huang,[a] Xiting Wang,[c] Huan Niu,[c] Yuzheng Guo, [c] Baikui Li,[a] Ruisheng Zheng,[a] Honglei Wu[a,*]

a College of Physics and Optoelectronic Engineering, Shenzhen University, Shenzhen, 518060, China;

b Department of Engineering, University of Cambridge, Cambridge, CB2 1PZ, United Kingdom;

c School of Electrical Engineering, Wuhan University, Wuhan, 430072, China.

# Contributed equally to this work.

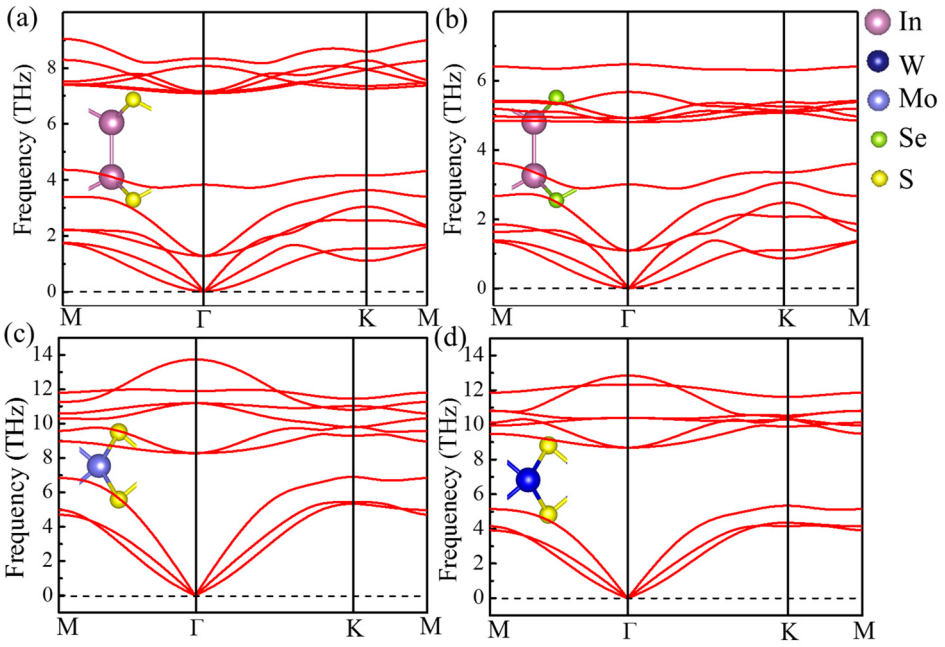

Fig. S1 The photon dispersions of (a) InS, (b) InSe, (c) MoS_2 and (d) WS_2 monolayer, respectively. The corresponding atomic unit cell is inserted.

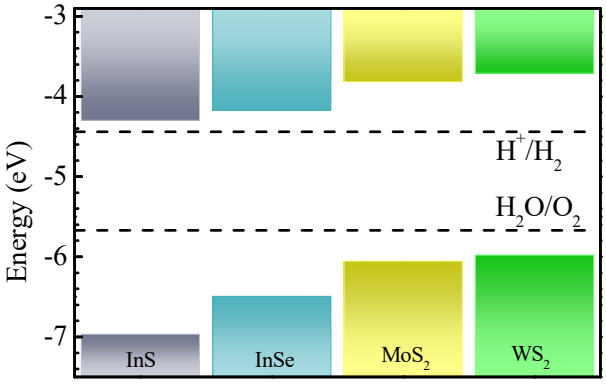

Fig. S2 Band edge positions of the InS, InSe, MoS_2 and WS_2 monolayers referring to the vacuum level. The redox potentials of water are labeled by black dotted lines.

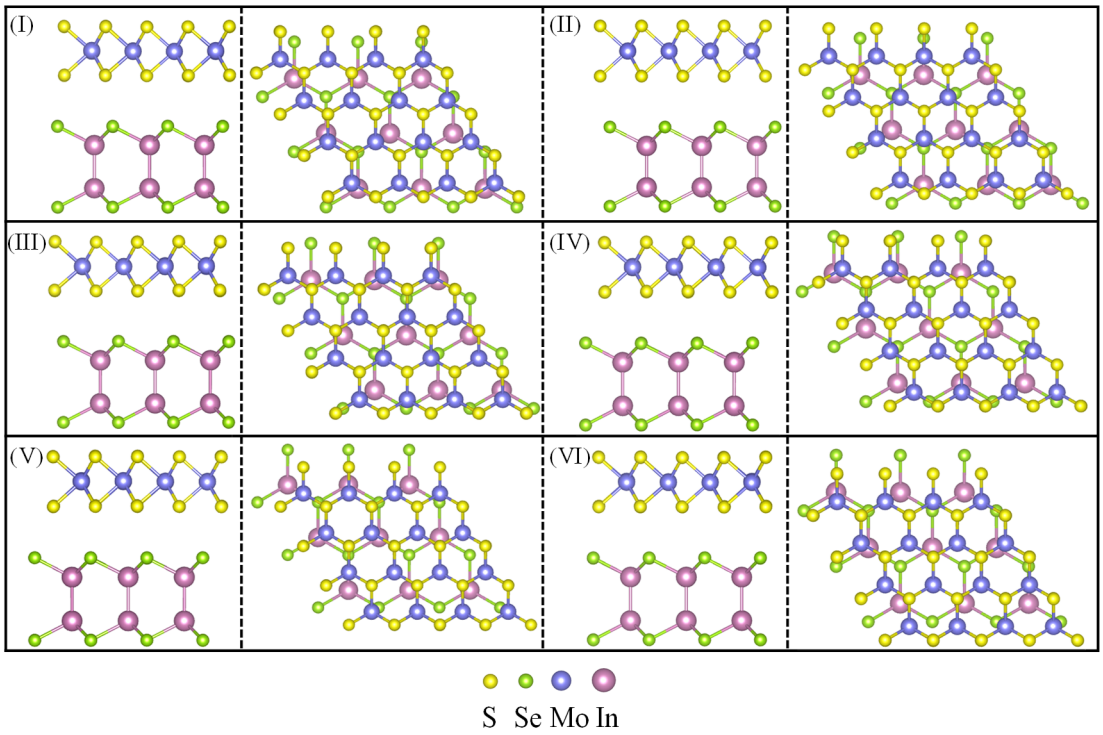

Fig. S3 Top and side views of the six stacking patterns of $InSe/MoS_2$. (a)-(f) is labeled as Stack-I to Stack-VI, respectively. The left panels are the side views and the right panels are the tops views. The same modeling is also appliable for the InS/MoS_2, InS/WS_2 and $InSe/WS_2$ heterostructures.

According to the relative atomic arrangement of the InSe and MoS_2 monolayers, we have constructed six different stacking patterns: S atoms of MoS_2 locate above the hexagonal ring center of InSe (labeled as Stack-I, Stack-II, and Stack-III), and Mo atoms of MoS_2 locate above the hexagonal ring center of InSe (labeled as Stack-IV, Stack-V, and Stack-VI). The detailed heterostructure models are shown in Fig. S3.

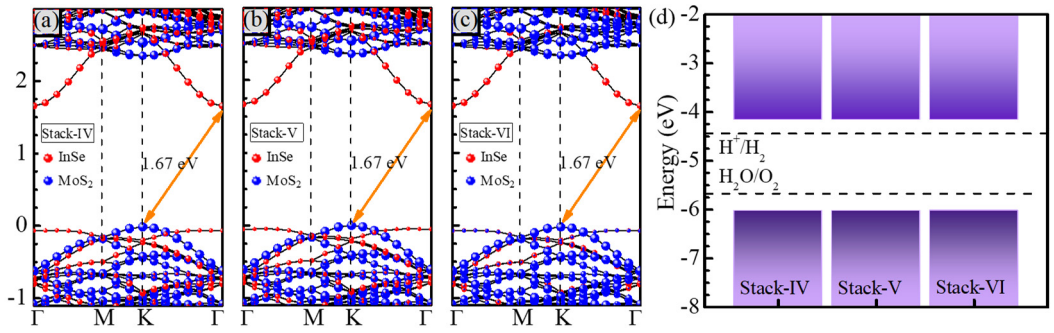

Fig. S4 Band structures of the InSe/MoS_2 heterostructure with (a) Stack-IV, (b) Stack-IV and (c) Stack-IV pattern; (d) shows the corresponding band edge positions.

As shown in Fig. S4, the band gap of the chosen stacking patterns are all ~1.67 eV and the difference is only within 0.0004 eV. Moreover, the band edge positions are also almost the same. Since the band gap values and band edge positions are two vital factors impacting photocatalytic ability, such negligible differences mentioned above do not impact the photocatalytic activity. The Stack-VI pattern is the most stable one, and hence it is selected as the studied pattern.

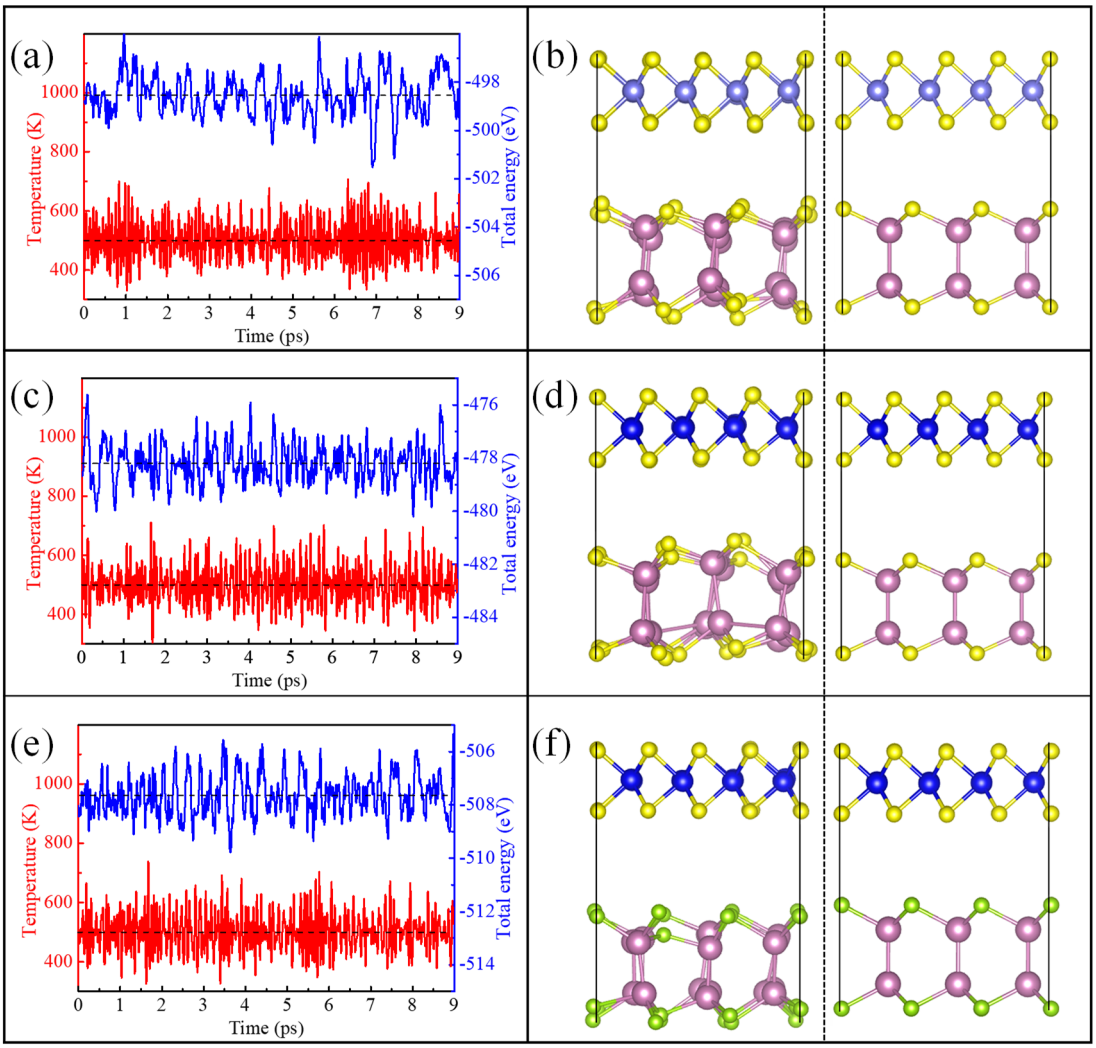

Fig. S5 (a) Evolution of temperature (red, left axis) and total energy (blue, right axis) with time during AIMD simulation for (a) InS/MoS_2, (c) InS/WS_2 and (e) $InSe/WS_2$ heterostructure, respectively. Atomic structures of the (b) InS/MoS_2, (d) InS/WS_2 and (f) $InSe/WS_2$ after 9 ps AIMD at 500 K (the left side) and further geometry relaxation (the right side)

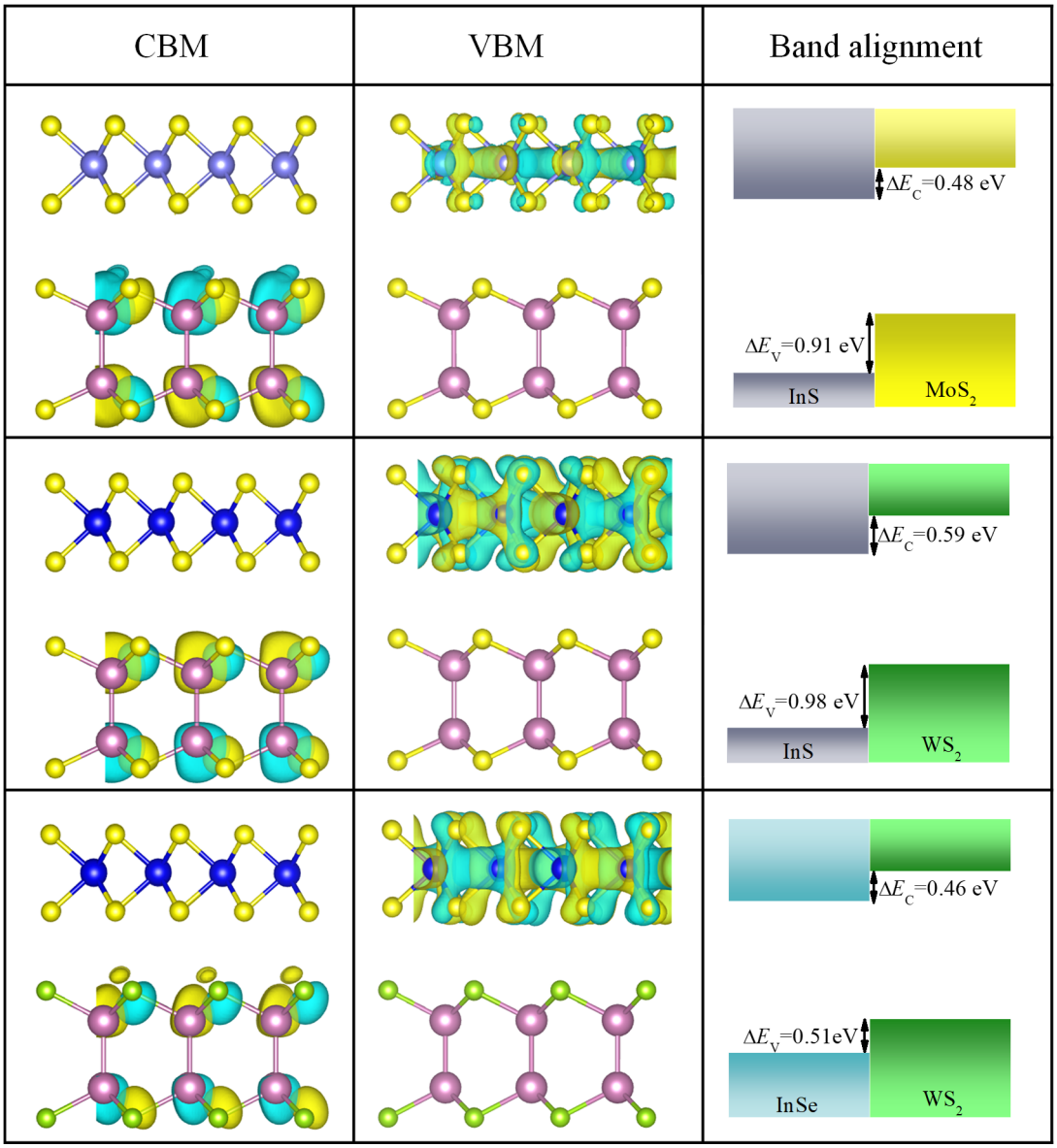

Fig. S6 Wavefunctions of CBM and VBM for InS/MoS_2, InS/WS_2 and InSe/WS_2 heterostructures (from top to bottom), and the corresponding band alignment diagrams. All the heterostructures show the type-II band alignment.

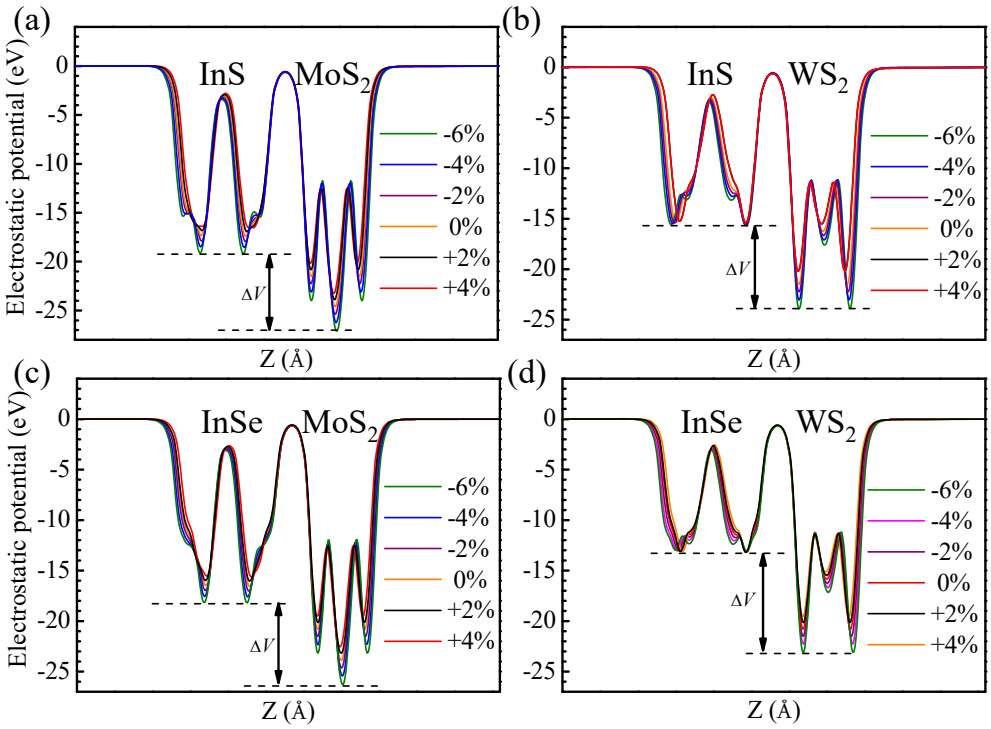

Fig. S7 The electrostatic potential of (a) InS/MoS_2, (b) InS/WS_2, (c) InSe/MoS_2, and (d) InSe/WS_2 heterostructures, respectively.

Table S1 The hole mobilities along x and y directions are listed together with the associated coefficients for monolayers and heterostructures. m^* (m_0), E_1 (eV), C_{2D} (J/m^2) and μ_{2D} (cm^{2}V^{-1}S^{-1}) represent effective mass, deformation potential constant, in-plane stiffness C_{2D}, and mobilities, respectively.

Materials	m_x^*	m_y^*	E_{1x}	E_{1y}	C_{2D-x}	C_{2D-y}	μ_x	μ_y
InS	1.89	1.76	1.61	1.79	45.07	44.81	107.34	92.98
InSe	1.98	1.68	1.32	1.97	48.86	48.77	165.89	87.99
MoS_2	0.63	0.62	6.09	6.34	138.31	140.43	201.76	193.92
WS_2	0.53	0.43	5.19	5.40	145.79	148.51	456.47	529.29
InS/MoS_2	1.35	1.38	3.62	3.91	180.93	182.84	159.85	135.46
InS/WS_2	1.23	1.19	3.83	4.18	188.62	191.89	184.35	162.74
InSe/MoS_2	1.37	1.23	3.71	4.03	182.31	185.89	158.89	152.93
InSe/WS_2	1.22	1.15	3.48	4.23	189.53	192.21	231.05	168.24

Table S2 Values used for the entropy and zero-point energy corrections in determining the free energy of reactants, products, and intermediate species adsorbed on catalysts[1]. For the adsorbates, the *ZPE* values are averaged over all single-atom catalyst systems since they have rather close values.

Species	*T***S* (eV) (298 K)	*ZPE* (eV)
O*	0	0.08
OH*	0	0.32
OOH*	0	0.42
H_2O(g)	0.58	0.57

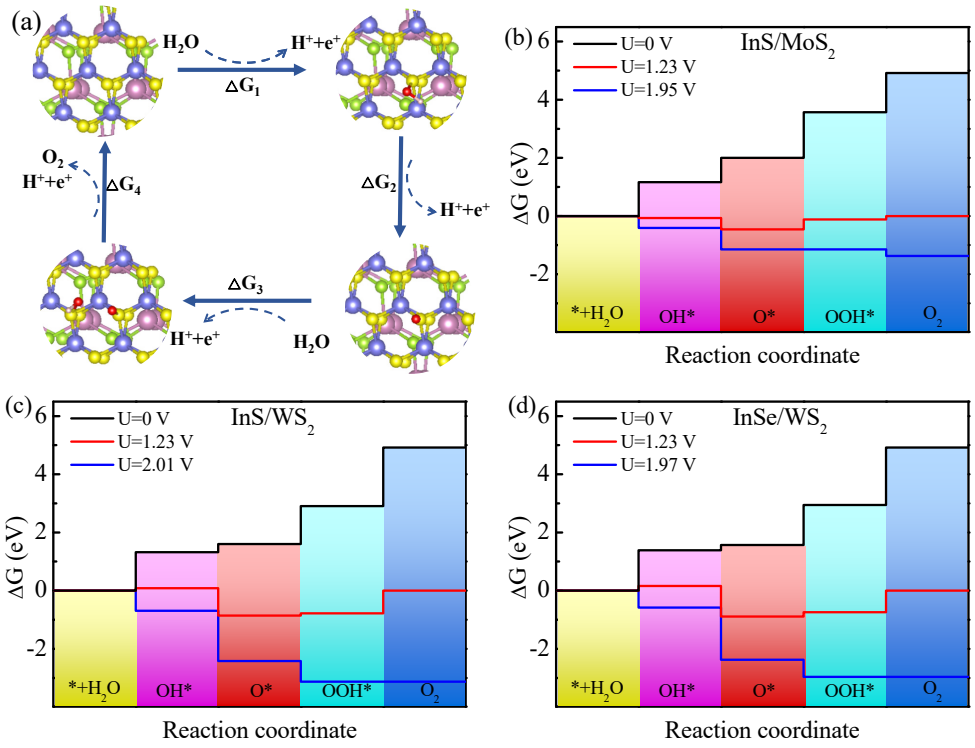

Fig. S8 (a) Proposed photocatalytic pathways of oxygen evolution reductions with the most energetically favorable absorbed intermediates (OH*, O*, OOH*). Free energy diagrams for the 4e pathways of oxygen evolution reductions in (b) InS/MoS_2, (c) InS/WS_2 and (d) InSe/WS_2 heterostructures, respectively.

Note S1

To compute the free energy change (ΔG) of each energy step in the water oxidation reactions, the model developed by Nørskov *et al* are adopted in this article, and the ΔG of an electrochemical reaction is determined as [2-4],

$$\Delta G=\Delta E+\Delta ZPE-T\Delta S \quad \text{(S1)}$$

where ΔE is the computed reaction energy, ΔZPE and ΔS are the zero-point energy difference and the entropy difference between the adsorbed state and the gas phase, respectively, and T is the system temperature. Herein, the ZPE of each adsorbate and free molecule can be attained by summarizing vibrational frequencies overall normal modes ν ($ZPE=1/2\sum h\nu_i$), while the zero-point energy of adsorption sites is negligible. All the ZPE and S results are shown in Table S2. The entropies of the free molecules (O_2, H_2O) were taken from the standard tables in Physical Chemistry.

The OER processes following the four-electron pathways, which can be expressed as:

$$*OH \rightarrow *O+(H^+ + e^-)$$

$$*+H_2O \rightarrow *OH+(H^+ + e^-)$$

$$*O+H_2O \rightarrow *OOH+(H^+ + e^-)$$

$$*OOH \rightarrow * + O_2+(H^+ + e^-)$$

where * indicates the active site on the surface of heterostructures. The absorption states of OH*, O*, and OOH* intermediates on InSe/MoS_2 heterostructure are also depicted in Fig. S7. The change of free energy (ΔG) is calculated with the following formula:

$$\Delta G=\Delta E+\Delta ZPE-T\Delta S-\Delta G_U-\Delta G_{pH}$$

where G, E, ZPE, and TS are the free energy, the total energy from the DFT calculation, the zero-point energy, and the entropic contribution, respectively. ΔG_U=-eU represents the effect of potential bias involving the electrode, where e is the elementary positive charge and U is the potential measured relative to the normal hydrogen electrode.

And the free energy change for OER electrochemical steps can be expressed as:

$$\begin{aligned}
\Delta G_1 &= G_{\mathrm{OH}^*} + 1/2G_{H_2} - G_{H_2O} - G^* \text{-} 0.059 \times pH - eU \\
\Delta G_2 &= G_{\mathrm{O}^*} + 1/2G_{H_2} - G_{OH^*} - 0.059 \times pH - eU \\
\Delta G_3 &= G_{\mathrm{OOH}^*} + 1/2G_{H_2} - G_{H_2O} - G_{O^*} - 0.059 \times pH - eU \\
\Delta G_4 &= 2G_{\mathrm{H_2O}} + G^* - 3/2G_{H_2} - G_{\mathrm{OOH}^*} + 4.92 - 0.059 \times pH - eU
\end{aligned} \tag{S2}$$

References

1 H. Xu, D. Cheng, D. Cao and X. C. Zeng, *Nat. Catal.*, 2018, 1, 339-348.

2 J. K. Nørskov, J. Rossmeisl, A. Logadottir, L. Lindqvist, J. R. Kitchin, T. Bliggard and H. Jónsson, *J. Phys. Chem. B*, 2004, 108, 17886-17892.

3 J. Rossmeisl, Z. W. Qu, H. Zhu, G. J. Kroes and J. K. Nørskov, *J. Electroanal. Chem.*, 2008, 607, 83-89.

4 A. Valdes, Z. W. Qu, G. J. Kroes and J. K. Nørskov, *J. Phys. Chem. C*, 2018, 26, 9872-9879.